21

Glucose-Induced Optical Clearing Effects in Tissues and Blood

Elina A. Genina, Alexey N. Bashkatov

Institute of Optics and Biophotonics, Saratov State University, Saratov, 410012, Russia

Valery V. Tuchin

Institute of Optics and Biophotonics, Saratov State University, Saratov, 410012, Russia,
Institute of Precise Mechanics and Control of RAS, Saratov 410028, Russia

This chapter describes tissue and blood optical clearing effects induced by action of glucose solutions. The main mechanisms of glucose-induced optical clearing are discussed. Tissue permeation for glucose, glucose delivery, tissue dehydration and swelling caused by glucose solutions are considered. Optical models of tissues and blood are presented. Optical clearing properties of fibrous (eye sclera, skin dermis and *dura mater*) and cell-structured tissues (liver) are analyzed using spectrophotometry, time- and frequency-domain, fluorescence and polarization measurements; confocal microscopy; two-photon excitation imaging; and OCT. *In vitro, ex vivo*, and *in vivo* studies of a variety of human and animal tissues, as well as cells and blood, are presented.

Key words: glucose, optical clearing, permeation, spectroscopy, fibrous tissues, cells, blood.

21.1 Introduction

Over the last decade, noninvasive or minimally invasive spectroscopy and imaging techniques have obtained wide spread occurrence in biomedical diagnostics, for example, optical coherence tomography (OCT) [1–4], visible and near-infrared elastic-scattering spectroscopy [4–7], fluorescent [1, 5, 8] and polarization spectroscopy [4, 9, 10] and others. The use of optical methods in the development of noninvasive clinical functional cerebral imaging systems for physiological-condition monitoring [11–13], intracranial hematoma and cancer diagnostics [14–16] can be alternative of conventional X-ray computed tomography, magnetic resonance imaging and ultrasound imaging [17–20] due to their simplicity, safety and low cost. Spectroscopic techniques are capable of deep-imaging of tissues that could provide information of blood oxygenation [21, 22] and detect cutaneous and breast tumours [10, 22], whereas confocal microscopy [23, 24], OCT [1–4] and multi-photon excitation imaging [24, 25] have been used to show cellular and sub-cellular details of superficial living tissues. Spectroscopic and OCT techniques are applicable for blood glucose monitoring with diabetic patients [4, 26–28] (see also chapters 3–10 and 18). Besides diagnostic applications, optical methods are widely used in therapy, for example, for photodynamic [29, 30] and laser interstitial thermotherapy [31], and for laser surgery of different diseases [32, 33]. In particular, in ophthalmology laser technology is used for transscleral photocoagulation of ciliary body [34, 35].

However, in spite of numerous benefits in the use of optical methods in medicine there are some serious disadvantages. One of the problems deals with the transport of the light beam through the turbid tissues, such as skin, eye sclera, cerebral membrane (*dura mater*), to the target region of the investigation or damage. Due to low absorption and comparatively high scattering of visible and NIR radiation at propagation within tissues, there are essential limitations on spatial resolution and light penetration depth for optical diagnostic and therapeutic methods to be successfully applied. In addition complex character of light interaction with the superficial tissue layers caused by tissue scattering properties modifies spectral and angular characteristics of light propagating within a tissue which may be a reason for false diagnostics or light dosimetry at therapeutic action [4, 36].

The evident solution of the problem is the reduction of light scattering by a tissue, which gives improvement of image quality and precision of spectroscopic information, decreasing of irradiating light beam distortion and its sharp focusing. Various physical and chemical actions, such as compression, stretching, dehydration, coagulation, UV irradiation, exposure to low temperature and impregnation by biocompatible chemical solutions, gels and oils, are widely described in literature as tools for controlling of tissue optical properties [4, 11]. All these phenomena can be understood if tissue is considered as a scattering medium that shows all optical effects that are characteristic to turbid physical systems. In general, the scattering properties of a tissue can be effectively controlled by providing matching refractive indices of the scatterers and the ground material (*i.e.*, optical immersion) and/or by the change

packing parameter, and/or scatterer sizing [4].

Aqueous glucose solutions are widely used for the control of tissue scattering properties [37–65]. Increase of glucose content in tissue interstitial space reduces refractive index mismatch and, correspondingly, decreases the scattering coefficient. At the same time, the increase of scatterer's volume fraction caused by dehydration of tissues may partly compensate the immersion effect. This chapter describes tissue and blood optical clearing effects induced by action of glucose solutions. *In vitro, ex vivo* and *in vivo* studies of a variety of human and animal tissues, such as fibrous (eye sclera, skin dermis and *dura mater*) and cellular tissues (liver), as well as cells and blood, are presented.

21.2 Structure and Optical Properties of Fibrous Tissues and Blood

21.2.1 Structure, physical and optical properties of fibrous tissues

Fibrous tissues, such as sclera, dermis and cerebral membrane (*dura mater*), show similar structure and, consequently, similar optical properties. These tissues consist mainly of conjunctive collagen fibers packed in lamellar bundles [4, 40, 66–68] that are immersed in an amorphous ground (interstitial) substance, a colorless liquid containing proteins, proteoglycans, glycoproteins and hyaluronic acid [69]. Fibrils are arranged in individual bundles in a parallel fashion; moreover, within each bundle, the groups of fibers are separated from each other by large empty lacunae distributed randomly in space. Collagen bundles show a wide range of widths (1 to 50 μm) and thicknesses (0.5 to 6 μm) [40, 66, 67]. These ribbon-like structures are multiple cross-linked; their length can be a few millimeters. They cross each other in all directions but remain parallel to the tissue surface. The glycosaminoglycans play a key role in regulating the assembly of collagen fibrils and tissue permeability to water and other molecules [70, 71]. It should be noted that these molecules are excellent space filters. Due to glycosaminoglycan chains, these molecules concentrate negative charges. They are highly hydrophilic, and their presence can provide a selective barrier to the diffusion of inorganic ions and charged molecules [69].

In spite of similarity of the fibrous tissues, some differences in their structure are caused by their different functions in an organism. This requires to overview briefly main features of the structure of these tissues.

The sclera is the turbid nontransparent medium that covers about 80% of the eyeball and serves as a protective membrane. Together with the cornea, it allows the eye to withstand both internal and external forces to maintain its shape. The thickness of the sclera is various. It is thicker at the posterior pole (0.9 to 1.8 mm); it is thinnest at the equator (0.3–0.9 mm) and at the limbus is in the range of 0.5 to 0.8 mm [4, 40, 72].

Hydration of the human sclera can be estimated as 68%. About 75% of its dry

weight is due to collagen, 10% is due to other proteins and 1% to mucopolysaccharides [72].

The sclera contains three layers: the episclera, the stroma and the *lamina fusca* [4]. At the *in vivo* investigations, it is necessary to take into account the presence of the conjunctiva and Tenon's capsule ($\sim 200\ \mu$m in thick), which both cover the scleral tissue from the external side. They impede the immersion liquid penetration into the sclera and, consequently, decrease the degree of eye tissue clearing. The thickness of the scleral collagen fibers also shows regional (limbal, equatorial and posterior pole region) and aging differences. In the equatorial region of the eye collagen fibrils exhibit a wide range of diameters, from 25 to 230 nm. The fibers in the scleral stroma have a diameter ranging from 30 to 300 nm [72]. The average diameter of the collagen fibrils increases gradually from about 65 nm in the innermost part to about 125 nm in the outermost part of the sclera [40, 72]; the mean distance between fibril centers is about 285 nm [73].

The episclera has a similar structure with more randomly distributed and less compact bundles than in the stroma. The *lamina fusca* contains a larger amount of pigments, mainly melanin, which are generally located between the bundles. The sclera itself does not contain blood vessels but has a number of channels that allow arteries, veins and nerves to enter or leave the eye [72].

Human *dura mater* is a protective membrane which surrounds brain. As an object for light propagation, this is a turbid, nontransparent medium. Typically, with the age the *dura mater* thickness changes from 0.3 to 0.8 mm [68, 74]. The average diameter of the *dura mater* collagen fibrils is about 100 nm [60].

Dura mater contains five layers: the external integumentary layer, the external elastin network, the collagen layer, the internal elastin network and the internal endothelium integumentary layer [68]. The collagen layer is the main layer of human *dura mater*. Thus, its optical properties are defined mainly by the optical properties of the collagen layer. It should be noted that those abrupt boundaries between upper, middle and lower layers are absent. The main difference between the structure of sclera and *dura mater* is the presence of the branched net of blood vessels in *dura mater* [68].

21.2.2 Structure, physical and optical properties of skin

Skin presents a complex heterogeneous medium where blood and pigment content are spatially distributed variably in depth [75–78]. Skin consists of three main visible layers from surface: epidermis (50–200 μm thick, the blood-free layer), dermis (1–4 mm thick, vascularized layer) and subcutaneous fat (from 1 to 6 mm thick depending on the body site). The randomly inhomogeneous distribution of blood and various chromophores and pigments in skin produces variations of average optical properties of skin layers. Nonetheless, it is possible to define the regions in the skin, where the gradient of skin cell structure, chromophores or blood amount change with a depth equals roughly zero [78]. This allows subdividing these layers into sublayers regarding the physiological nature, physical and optical properties of their cells and pigments' content. The epidermis can be subdivided into the two sublayers: nonliv-

ing and living epidermis. Nonliving epidermis or *stratum corneum* (about 10–20 μm thick) consists of only dead squamous cells, which are highly keratinized with a high lipid and protein content, and has a relatively low water content [76, 78, 79]. Living epidermis (50–200 μm thick) contains most of the skin pigmentation, mainly melanin, which is produced in the melanocytes [80].

Physical and optical properties of the dermal layers are mainly defined by the fibrous structure of the tissue. Dermis is a vascularized layer and the main absorbers in the visible spectral range are the blood hemoglobin, carotene and bilirubin. Following the distribution of blood vessels [77] skin dermis can be subdivided into the four layers: the papillary dermis ($\sim$ 150 μm thick), the upper blood net plexus ($\sim$ 100 μm thick), the reticular dermis (1–4 mm thick) and the deep blood net plexus ($\sim$ 100 μm thick).

In fibrous tissues light scatters by both single fibrils and scattering centers, which are formed by the interlacement of the collagen fibrils and bundles. The average scattering properties of the skin are defined by the scattering properties of the reticular dermis because of relatively big thickness of the layer (up to 4 mm [79]) and comparable scattering coefficients of the epidermis and the reticular dermis. Large melanin particles such as melanosomes ($>$ 300 nm in diameter) exhibit mainly forward scattering. Whereas melanin dust whose particles are small ($<$ 30 nm in diameter) has the isotropy in the scattering profile, and optical properties of the melanin particles (30–300 nm in diameter) may be predicted by the Mie theory.

Absorption of hemoglobin and water in skin dermis and lipids in skin epidermis define absorption properties of whole skin. It should be noted that absorption of hemoglobin is defined by the hemoglobin oxygen saturation, since absorption coefficients of hemoglobin are different for oxy and deoxy forms. For an adult the arterial oxygen saturation is generally above 95% [81]. Typical venous oxygen saturation is 60–70% [82]. Thus, absorption properties of skin in the visible spectral range depend on absorption of both oxy- and deoxyhemoglobin. In the IR spectral range absorption properties of skin dermis depend on absorption of water.

To design the optical model of fibrous tissue, in addition to form, size and density of the scatterers (collagen fibrils) and the tissue thickness, we are able to have information on the refractive indices of the tissue components. In the visible and near infrared spectral ranges, the refractive index of collagen fibrils and interstitial fluid (ISF) of human tissues has a weak dispersion and, thus, in a first approximation, can be used as a constant. The experimental mean values of refractive indices of tissues, blood and their compounds, measured *in vitro* and *in vivo*, have been presented [4, 65, 83].

21.2.3 Optical model of fibrous tissue

The optical model of fibrous tissue can be presented as a slab with a thickness l containing scatterers (collagen fibrils) – thin dielectric cylinders with an average diameter of 100 nm, which is considerably smaller than their lengths. Taking into account the similar structure of the *dura mater*, eye sclera and skin dermis, we can assume that the refractive index of the collagen fibrils (n_c) and ISF (n_I) has the

similar wavelength dependence in the visible spectral range for all fibrous tissues [60].

$$n_c(\lambda) = 1.439 + \frac{15880.4}{\lambda^2} - \frac{1.48 \times 10^9}{\lambda^4} + \frac{4.39 \times 10^{13}}{\lambda^6} \tag{21.1}$$

and

$$n_I(\lambda) = 1.351 + \frac{2134.2}{\lambda^2} + \frac{5.79 \times 10^8}{\lambda^4} - \frac{8.15 \times 10^{13}}{\lambda^6}, \tag{21.2}$$

where λ is the wavelength, nm.

These cylinders are located in planes that are in parallel to the sample surfaces, but within each plane their orientations are random. These simplifications reduce considerably the difficulties in the description of the light scattering by fibrous tissue. For a thin dielectric cylinder in the Rayleigh-Gans approximation of the Mie scattering theory the scattering cross-section $\sigma_s(t)$ for unpolarized incident light is given by [84, 85]

$$\sigma_s = \frac{\pi^2 a x^3}{8} \left(m^2 - 1\right)^2 \left(1 + \frac{2}{\left(m^2 + 1\right)^2}\right), \tag{21.3}$$

where $m = n_c/n_I$ is the relative refractive index of the scattering particle, *i.e.*, ratio of the refractive indices of the scatterers and the ground materials (*i.e.*, ISF), and x is the dimensionless relative scatterers size which is determined as $x = 2\pi a n_I/\lambda$, where λ is the wavelength and a is the cylinder radius.

Considerable refractive indices mismatching between collagen fibers and a ground substance causes the system to become turbid, *i.e.*, causes multiple scattering and poor transmittance of propagating light. The refractive index of the background is a controlled parameter and may transit the system from multiple to low-step and even single-scattering mode. For $n_c = n_I$, the medium becomes totally homogeneous and optically transparent if absorption is negligible.

The temporal dependence of the refractive index of the ISF caused by the clearing agent permeation into a tissue can be derived using the law of Gladstone and Dale, which states that for a multi-component system the resulting value of the refractive index represents an average of the refractive indices of the components related to their volume fractions [86, 87]. Such dependence is defined as

$$n_I(t) = [1 - C(t)]\, n_{\text{base}} + C(t)\, n_{\text{osm}}, \tag{21.4}$$

where n_{base} is the refractive index of the tissue ISF at the initial moment and n_{osm} is the refractive index of an agent solution. In practice any of the available optical clearing agents (OCAs) can be taken to provide light scattering reduction [65]; however in this chapter the advantages of the glucose solution will be considered. Wavelength dependence of aqueous glucose solution can be estimated as [63]

$$n_{\text{osm}}(\lambda) = n_w(\lambda) + 0.1515C, \tag{21.5}$$

where $n_w(\lambda)$ is the wavelength dependence of the refractive index of water [88], and C is the glucose concentration, g/ml.

As a first approximation we assume that during the interaction of the immersion liquid with a tissue, the size of the scatterers does not change. This assumption is confirmed by the results presented by Huang and Meek [89] for scleral and corneal tissue at action of polyethylene glycol solutions at pH values near 4. In the case of unchangeable scatterer size, all changes in the tissue scattering are connected with the changes of the refractive index of the ISF described by Eq. (21.1). The increase of the refractive index of the ISF provides the decrease of the relative refractive index of the scattering particles and, consequently, the decrease of the scattering coefficient. For noninteracting particles the scattering coefficient of a tissue is defined by the following equation

$$\mu_s(t) = N\sigma_s(t), \tag{21.6}$$

where N is the number of the scattering particles (fibrils) per unit area and $\sigma_s(t)$ is the time-dependent cross-section of scattering [Eq. (21.3)]. The number of the scattering particles per unit area can be estimated as $N = \phi/(\pi a)^2$ [84], where ϕ is the volume fraction of the tissue scatterers. For fibrous tissues ϕ is usually equal to 0.3 [36, 40, 90].

To take into account interparticle correlation effects, which are important for tissues with densely packed particles, the scattering cross-section has to be corrected by the packing factor of the scattering particles, $(1-\phi)^3/(1+\phi)$ [36]. Thus, Eq. (21.6) has to be rewritten as

$$\mu_s(t) = \frac{\phi}{\pi a^2}\sigma_s(t)\frac{(1-\phi)^3}{1+\phi}. \tag{21.7}$$

Tissue swelling (or shrinkage) caused by action of an OCA leads to change of tissue sample volume that produces the corresponding change of the volume fraction of the scatterers and their packing factor, as well as the numerical concentration, *i.e.*, the number of the scattering particles per unit area.

21.2.4 Structure, physical and optical properties of blood

From an optical point of view, whole blood is a highly concentrated turbid medium consisting of plasma (55–60 vol%) and blood particles (40–45 vol%) [91, 92], 99% of which are erythrocytes and 1% are leukocytes and platelets [92].

In normal physiological conditions human erythrocytes (red blood cells – RBCs) are anucleate cells in the form of biconcave disks with a diameter ranging between 5.7 and 9.3 μm and mean size of about 7.5 μm [92], and maximal thickness varying between 1.7 and 2.4 μm [93]. Average volume of a RBC is about 90 μm^3 [91, 94, 95] and, according to different data, varies between 70 and 100 μm^3 [93], from 50 to 200 μm^3 [94] or from 30 to 150 μm^3 [95]. In the presence of different pathologies, as well as under changes of osmolarity or pH of the blood plasma, the normal (discocytes) can change shape without changing in volume [92, 93]. The RBCs consist

of a thin membrane (with a thickness from 7 nm [94] to 25 nm [93]) and cytoplasm, which, in general, is an aqueous hemoglobin solution [95, 96].

Hematocrit is the volume fraction of cells within the whole blood volume and ranges from 36.8% to 49.2% under physiological conditions [91]. The hemoglobin concentration in completely hemolyzed blood lies between 134 and 173 g/L [91], while the hemoglobin concentration in erythrocytes varies from 300 to 360 g/L, with mean concentration being equal to 340 g/L [95]. The content of salts in the erythrocyte cytoplasm is about 7 g/L, and concentration of other organic components (lipids, sugars, enzymes and proteins) is approximately equal to 2 g/L [96]. A change in osmolarity induces a variation of the RBC volume due to water exchange and therefore has an impact on the hemoglobin concentration within the RBC [91].

Flow induced shear stress can influence RBC sedimentation, their reversible agglomeration, axial migration or deformation, and orientation. The flow parameters depend on the blood viscosity and they are influenced by the fact that blood is not a Newton fluid [91, 96].

Under normal physiological conditions, the RBCs may aggregate into rouleaux. The rouleaux may further interact with other rouleaux to form rouleaux networks (or clumps in pathological cases) [91, 93, 96].

21.2.5 Optical model of blood

The optics of whole blood at physiological conditions is determined mainly by the optical properties of RBCs and plasma, whereas the contribution to scattering from the remaining blood particles can be neglected. Analysis of light propagation and scattering in such medium can be performed on the basis of description of absorption and scattering characteristics of individual blood particles by taking into account concentration effects and polydispersity of the particles.

In radiative transfer theory the absorption coefficient μ_a, scattering coefficient μ_s and anisotropy factor g of an elementary volume of investigated medium are determined by the size of RBCs, as well as real (n) and imaginary (χ) parts of the complex refractive index $(n + i\chi)$ of the scattering particles (RBCs) and their environment (blood plasma). The scattering properties of blood are also dependent on RBC volume, shape and orientation, which are defined in part by blood plasma osmolarity [91], aggregation and disaggregation capability and hematocrit [97].

In the blood optical model, scattering particles can be represented as absorbing and scattering homogeneous spherical particles with volume of each particle being equal to the volume of a real RBC [98, 99]. Contribution to the scattering from the RBC membrane can be neglected due to small thickness of the membrane [95]. Polydispersity of RBCs can be taken into account based on the data presented in Ref. [94].

According to the data obtained in Ref. [95], the concentration of hemoglobin can be related to the RBC volume as:

$$C_{\mathrm{Hb}} = 0.72313 - 0.00451V, \tag{21.8}$$

where C_{Hb} is the concentration of hemoglobin, g/ml, and V is the erythrocyte volume, $\mu\mathrm{m}^3$.

Both the real and the imaginary parts of the refractive index of erythrocytes are directly proportional to the hemoglobin concentration in erythrocytes [91, 92], *i.e.*:

$$n_e = n_0 + \alpha C_{\mathrm{Hb}}, \tag{21.9}$$

$$\chi_e = \beta C_{\mathrm{Hb}}, \tag{21.10}$$

where $n_0 = 1.34$ is the refractive index of the erythrocyte cytoplasm [95] and α and β are spectrally dependent coefficients. For the wavelength of 589 nm, $\alpha = 0.1942$ ml/g [91], while, for the wavelength 640 nm, $\alpha = 0.284$ ml/g and $\beta = 0.0001477$ ml/g [92]. Since the content of salts, sugars and other organic components in the erythrocyte cytoplasm is insignificant, the spectral dependence of the erythrocyte cytoplasm correlates with the spectral dependence of the refractive index of water, *i.e.*, $n_0(\lambda) = n_w(\lambda) + 0.007$. Spectral dependence of the refractive index of water is determined in Ref. [88]. The spectral dependences of the coefficients α and β can be calculated on the basis of the data presented in Ref. [92] and using a value of the hemoglobin concentration in RBC equal to 322 g/l, which can be obtained from Eq. (21.9) with the coefficient $\alpha = 0.1942$ ml/g.

The blood plasma contains up to 91% water, 6.5–8% (about 70 g/l) proteins (hemoglobin, albumin and globulin) and about 2% low-molecular-weight compounds [61]. The spectral dependence of the real part of the refractive index of the blood plasma (n_p) in the spectral range 400–1000 nm is determined by the expression [64, 100]

$$n_p = 1.3254 + \frac{8.4052 \times 10^3}{\lambda^2} - \frac{3.9572 \times 10^8}{\lambda^4} - \frac{2.3617 \times 10^{13}}{\lambda^6}, \tag{21.11}$$

where λ is the wavelength (nm). Since the blood plasma does not have pronounced absorption bands in this spectral range, the imaginary part of the refractive index of the plasma can be neglected in calculations.

In terms of the Mie theory, the scattering (σ_s) and the anisotropy factor of a homogeneous sphere are expressed by Eqs. (19.37) and (19.38) of Ref. [85].

According to [36], the scattering and absorption coefficients and the anisotropy factor of whole blood considered as a system of closely packed polydisperse particles are given by

$$\mu_s = (1 - H) \sum_{i=1}^{M} N_i \sigma_{s_i}, \tag{21.12}$$

$$\mu_a = \sum_{i=1}^{M} N_i \sigma_{a_i}, \tag{21.13}$$

$$g = \sum_{i=1}^{M} \mu_{s_i} g_i \Big/ \sum_{i=1}^{M} \mu_{s_i}. \tag{21.14}$$

Here H is the hematocrit value; $M$is the number of volume fractions of erythrocytes; $N_i = C_i/V_{ei}$ is the number of particles per unit volume of the medium; C_i is the volume fraction occupied by particles of the ith diameter; $V_{ei} = 4\pi a_i^3/3$ is the erythrocyte volume. In Eq. (21.12) the necessity of introduction of the factor $(1 - H)$ [94, 101, 102], which is called the packing factor of scatterers, is determined by interference effects of radiation scattered by the neighboring particles.

21.3 Glucose-Induced Optical Clearing Effects in Tissues

21.3.1 Mechanisms of optical immersion clearing

Numerous publications discuss advantages of methods of tissue optical clearing using OCAs and investigation of the mechanisms of clearing [45, 47, 49, 54, 57, 60, 65, 103–106]. There are a few main mechanisms of light scattering reduction induced by an OCA [57, 65, 103–106]: 1) dehydration of tissue constituents, 2) partial replacement of the ISF by the immersion substance and 3) structural modification or dissociation of collagen. Both the first and the second processes mostly cause matching of the refractive indices of the tissue scatterers (cell compartments, collagen and elastin fibers) and the cytoplasm and/or ISF. Tissue dehydration and structural modification lead to tissue shrinkage, *i.e.*, to the near-order spatial correlation of scatterers and, as a result, the increased constructive interference of the elementary scattered fields in the forward direction and destructive interference in perpendicular direction of the incident light, that may significantly increase tissue transmittance even at some refractive index mismatch [65]. For some tissues and for nonoptimized pH of clearing agents, tissue swelling may take place that may be considered as a competitive process in providing of tissue optical clearing [65, 89].

It was shown that dehydration induced by osmotic stimuli such as OCA appears to be a primary mechanism of optical clearing in collagenous and cellular tissues, whereas dehydration induces intrinsic matching effect [65, 103]. The space between fibrils and cell organelles is filled up by water and suspended salts and proteins. Water escaping from tissue having cellular or fibrillar structure is a more rapid process than OCA entering into tissue interstitial space due to the fact that OCA typically has greater viscosity (lower diffusion coefficient) than water. As water is removed from the intrafibrillar or intracellular space, soluble components of ISF or cytoplasm become more concentrated and a refractive index increases. The resulting intrinsic refractive index matching between fibrils or organelles and their surrounding media, as well as density of packing and particle ordering, may significantly contribute to optical clearing [56, 65, 103]. Replacement of water in the interstitial space by the immersion substance leads to the additional matching of the refractive indices between tissue scatterers and ground matter [4, 56].

21.3.2 Optical clearing of fibrous tissues

21.3.2.1 *In vitro* spectral measurements

For *in vitro* studies of tissue optical glucose-induced clearing fiber optical grating-array spectrometer LESA-5, 6med (Biospec, Russia) or similar are suitable thanks to their fast spectra collection during glucose solution action [11, 41, 42, 44–52, 56–58, 60]. Typically, the spectral range of interest is from 400 to 1000 nm. For providing of measurements in transmittance mode the glass cuvette with the tissue sample was placed between two optical fibers. One fiber transmitted the excitation radiation to the sample, and another fiber collected the transmitted radiation. The 0.5-mm diaphragm placed 100 mm apart from the tip of the receiving fiber was used to provide collimated transmittance measurements [41, 44, 45, 49, 51, 60]. The tissue samples were fixed inside cuvette filled up with the glucose solution. In the reflectance mode the spectrometer fiber probe consists of seven optical fibers: one fiber delivers light to the object, and six fibers collect the reflected radiation [44, 46, 47, 51, 52, 57]. The same configuration was used also in *in vivo* investigations.

The total transmittance and diffuse reflectance were measured in the wavelength range 200-2200 nm using spectrophotometer with an internal integrating sphere Cary 2415 (Varian, Australia) [40, 43] or PC1000 (Ocean Optics Inc., USA) [59]. The spectrometers were calibrated using a white slab of $BaSO_4$ with a smooth surface. To reconstruct the absorption and reduced scattering coefficients of a tissue from the measurements, the inverse adding-doubling (IAD) [107] or inverse Monte Carlo (IMC) were applied [108].

Figures 21.1 and 21.2 illustrate dynamics of glucose-induced change of the transmittance spectra of two types of fibrous tissues: sclera and *dura mater*. In the figures symbols correspond to experimental data [42, 60], the error bars show the standard deviation values and the solid lines correspond to the data calculated using the optical model of fibrous tissue. It is easily seen that the untreated tissue is poorly transparent for the visible light. Administration of 40%- as well as 20%-glucose solutions makes fibrous tissue highly transparent. The approximated time of maximal tissue clearing is about 8 min.

Figures show that the clearing process has at least two stages. At the beginning of the process the increase of the transmittance is seen; that is followed by saturation and even the decrease of the transmittance. Two major processes could take place. One of them is diffusion of glucose inside tissue and another is tissue dehydration caused by osmotic properties of glucose. In general, both processes lead to matching of refractive indices of the scatterers and the ISF that causes the decrease of tissue scattering and, therefore, the increase of the collimated transmittance. Dehydration also leads to the additional increase of optical transmission due to decrease of tissue thickness (shrinkage) and corresponding scatterer ordering (packing in order) process due to increase of particle volume fraction. However, the increase of scatterer volume fraction may also cause some competitive increase of scattering coefficient due to random packing process (growth of particle density) that partly compensates the immersion effect. The saturation of optical clearing kinetic curves (see Figs. 21.1 and 21.2) can be explained as the saturation of glucose and water diffusion processes.

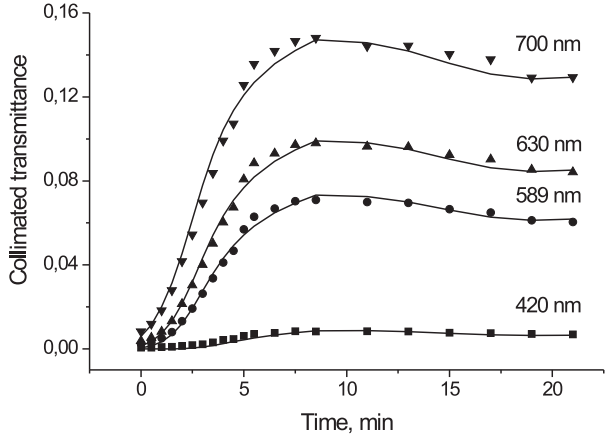

FIGURE 21.1: The time-dependent collimated transmittance of the human sclera sample measured *in vitro* at different wavelengths concurrently with administration of 40%-glucose solution. The symbols correspond to the experimental data. The solid lines correspond to the data calculated using the optical model of fibrous tissue [42].

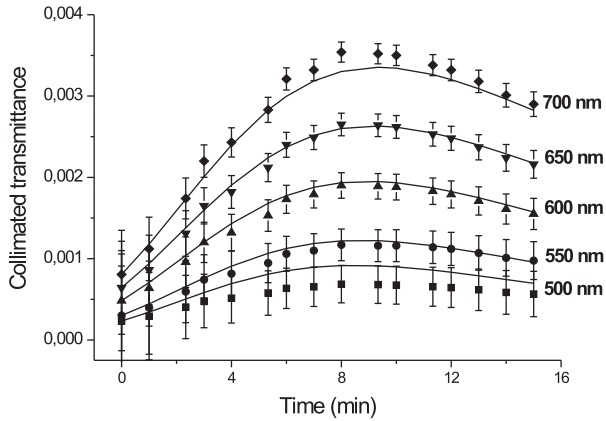

FIGURE 21.2: The time-dependent collimated transmittance of the human *dura mater* sample measured at different wavelengths concurrently with administration of 20%-glucose solution. The symbols correspond to the experimental data. The error bars show the standard deviation values. The solid lines correspond to the data calculated using the optical model of fibrous tissue [60].

Some darkening at the late time period may be caused by a few reasons, such as the above mentioned particle density growth and interaction of modified ISF (containing glucose and less water) with hydrated collagenous fibrils [65].

21.3.2.2 *In vivo* spectral measurements

It is known that at *in vivo* application of the designed optical immersion technology additional factors such as metabolic reaction of living tissue on clearing agent application, the specificity of tissue functioning and its physiological temperature can significantly change kinetic characteristics and the magnitude of the clearing effect. Temporal dependence of the sclera reflectance at two wavelengths in the course of the optical clearing of rabbit eye *in vivo* is presented in Fig. 21.3 [46]. As it was shown in *in vitro* studies [40, 41, 43], visible and NIR reflectance of scleral samples monotonically decreases under the action of the 40%-glucose solution, unlike *in vivo* measurements. The oscillatory character of kinetic curves is caused by the alternation of processes of clearing, which appears after the application of glucose solution to the eye surface (glucose solution drop), and recovery of the optical properties of sclera after diffusion of glucose from the detection region to surrounding tissues and diffusion of water from surrounding tissues to the detection region. Each oscillation corresponds to time of a new glucose drop applied topically.

The time during which the maximum transparency of sclera was achieved *in vivo* considerably exceeds the clearing time of sclera *in vitro*. While this time was 8–10 min upon the action of the 40%-glucose solution on sclera samples *in vitro* [40, 41, 43], the clearing processes during *in vivo* experiments proceeded for no less than 20 min. There are at least two reasons for that. In *in vitro* studies typically both sides of the samples are impregnated by a solution; in *in vivo* case glucose solution could be applied only from one side of a tissue at topical application. Another reason is that the upper cellular epithelial layer of the sclera may have some impact (hindering) on glucose diffusivity.

The kinetic curves measured for two wavelengths, one of which (568 nm) is within and another (610 nm) is outside the absorption band of blood (Fig. 21.3), are considerably different. The reflectance within blood absorption band decreased much faster (for 10–12 min) that is explained by the response of the eye (inflammation) to intense illumination during measurements as well as by the osmotic action of glucose. Such induced inflammation increases the local concentration of hemoglobin due to blood inflow through vessels. A further small increase in R in this wavelength range can be explained by a decrease in the absorption of light in sclera due to the stasis of capillaries and microvessels caused by the hyperosmotic action of glucose inside sclera [52]. This effect will be discussed below.

Since sclera is the tissue with low blood content, blood absorption practically does not become apparent in the spectra at *in vitro* measurements [40, 41, 43]. Therefore the reflectance demonstrates uniform falling due to the immersion clearing at all wavelengths. The appearance of the blood spectral bands at *in vivo* measurements is mainly connected with the existence of choroid under scleral layer, which is usually deleted at *in vitro* experiments, and functioning capillary net inside the sclera.

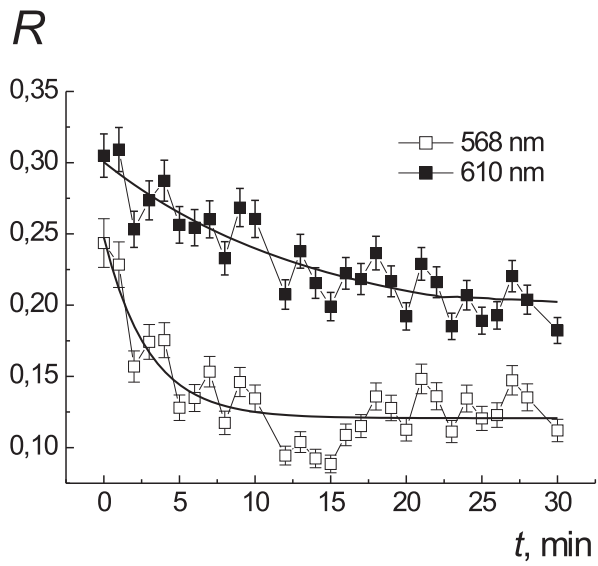

FIGURE 21.3: Temporal dependence of the sclera reflectance at two wavelengths during the optical clearing. Symbols and solid curves correspond to experimental data and result of their approximation, respectively [46].

The change of regime of photon scattering from multiple to low-step leads to the increase of photon's free path length. Thus, more photons pass the scleral layer almost without the scattering and are absorbed in choroid layer. This corresponds to more significant decreasing of the reflectance in the blood absorption bands in comparison with the range 600–750 nm. Besides, the action of osmotic agent causes the irritation of eyeball that causes more blood coming to the area under study and, thus, additionally reduces the reflectance of tissue in the range of blood absorption bands.

By numerical simulation of scleral optical clearing process under the action of the 40%-glucose solution, the time dependences of the fraction of absorbed photons in each layer of the eye cover (sclera, retinal pigmented epithelium and choroid) has been evaluated [46]. The fraction of photons absorbed in sclera decreases with time, on average, by 10%, in accordance with sclera clearing. The fraction of photons absorbed in retinal pigmented epithelium layer increases, on average, by 30%. The fraction of photons absorbed in the choroid increases by 40%. This means that, despite sclera clearing, the main part of light transmitted through sclera is absorbed in pigmented and vascular layers. As a result, the intensity of light incident on the internal tissues of the eye increases insignificantly. This should be taken into account in the dosimetry of laser radiation in transscleral surgery of the inner eye ball tissues because a considerable increase in the absorption of light in retinal pigmented epithelium and choroid layers at sclera clearing can cause their overheating and damage.

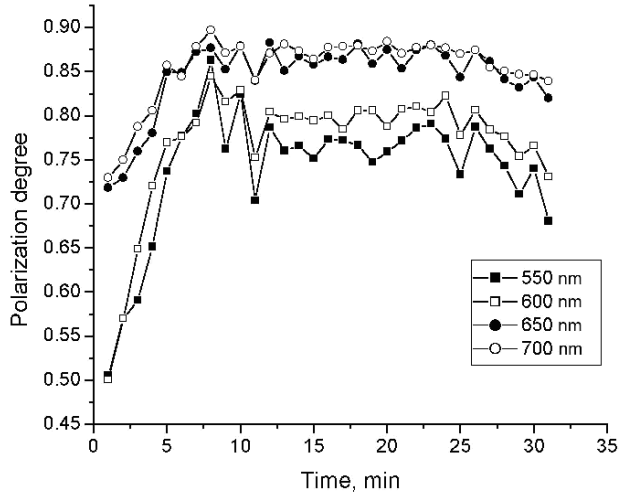

FIGURE 21.4: The time-dependent polarization degree $(I_{||} - I_{\perp})/(I_{||} + I_{\perp})$ of collimated transmittance measured at different wavelengths for the rabbit eye sclera sample at administration of 40%-glucose [41].

On the other hand, scleral optical clearing may provide more precise and effective coagulation of retinal pigmented epithelium and choroid layers [65].

21.3.2.3 Polarization measurements

The kinetics of the polarization properties of the tissue sample at immersion can be easily observed using an optical scheme with a white light source and a tissue sample placed between two parallel or crossed polarizers [41]. At a reduction of scattering, the degree of linearly polarized light propagating in fibrous tissue improves [11, 41, 109]. This is clearly seen from the experimental graphs in Fig. 21.4.

As far as the tissue is immersed, the number of scattering events decreases and the residual polarization degree of transmitted linearly polarized light increases. As a result, the kinetics of the average transmittance and polarization degree of the tissue are similar. It follows from Fig. 21.4 that glucose-induced optical clearing leads to increasing in the depolarization length [109]. Due to less scattering of the longer wavelengths, the initial polarization degree is higher for these wavelengths. Tissue clearing has the similar impact on scattering and correspondingly on the improvement of polarization properties on these long wavelengths and especially on the shorter ones.

21.3.3 Optical clearing of skin

21.3.3.1 Confocal microscopy

Skin has a principle limitation that makes the optical clearing method less efficient and more complicated to be applied and described. The origin of this limitation is the dense upper cellular layer *stratum corneum* (SC), which has a protective function preventing penetration of any chemicals including immersion agents inside the skin. The specific structure of skin defines the methods of its effective optical clearing.

The heterogeneous nature of skin provides some possible pathways for solute transport: appendageal, transcellular (through corneocytes) and intercellular (through the lipid phase — lipid bridges) [110]. Lipophilic solutes are permeants believed to be transported via the lipoidal pathway of SC and polar permeants are transported via the pore pathway of SC [111]. It is well known that the diffusion of aqueous solutions of substances (such as glucose) through SC barrier is hindered.

The main limitation of the confocal microscopy in skin studies is skin high scattering that distorts the quality of cell images. The increase in the transparency of the upper skin layers can improve the penetration depth, image contrast, and spatial resolution of confocal microscopy [53, 54]. At administration of an OCA to the skin superficial layers they are greatly cleared during the first minute of the process. It is connected mainly with a high porosity of the SC dead cell structure, where air-filled small spaces exist. In depth of SC, where very dense structure is formed by corneocytes that are attached to each other by lipid bridges, diffusion of any agent, including glucose and water, is dramatically reduced. Living epidermis cell layers are a few orders more permeative; however its thickness is 5–10 times bigger than of SC, thus the overall diffusion rate through SC and living epidermis may be comparable [58]. Skin dermis is characterized by a faster diffusion that is characteristic to any fibrous tissue. In the upper blood net plexus region permeability of dermis may be modified (typically fastened) due to blood and lymph vascular net structure [112]. In the deep skin layers OCA diffusion is more homogeneous. The diffusivity of glucose and water is a few orders higher than in living epidermis, and only a half of the order less than diffusion in water [65]. However, because of considerable thickness of dermis in comparison with SC and living epidermis the overall permeation could be comparable with permeation of SC and living epidermis.

Using Monte Carlo simulation of the point spread function it was shown recently that confocal microscopic probing of skin at optical clearing is potentially useful for deep *reticular dermis* monitoring and improving the image contrast and spatial resolution of the upper cell layers [54]. The results of the simulation predict that, to 20th min of glucose diffusion after its intradermal injection, a signal from layers located twice as deeply in the skin can be detected [53].

21.3.3.2 Two-photon microscopy

The application of glucose may prove to be particularly relevant for enhancing two-photon microscopy [113], since it has been shown that the effect of scattering is to drastically reduce penetration depth to less than that of the equivalent single pho-

ton fluorescence while largely leaving resolution unchanged [114, 115]. This happens mostly due to excitation beam defocusing (distortion) in the scattering media. On the other hand, this technique is useful in understanding molecular mechanism of tissue optical clearing upon immersion and dehydration [56].

For two-photon scanning fluorescence microscopy system, a mode-locked laser provides the excitation light. The fluorescence is collected by the objective and retraces the same optical path as the laser excitation. In Ref. [55] Ti:Sapphire laser (Coherent MIRA900) as a source of the excitation light, which comprises 100-fs width pulses at an 80-MHz repetition rate, tuneable in wavelength between 700 and 1000 nm, was used. The wavelength range of the detection has an upper limit of 670 nm, and a lower limit of 370 nm. Samples were taken from normal human skin excised during plastic surgery procedures. Images were taken at depths of 20, 40, 60 and 80 μm from the sectioned surface of the skin tissue.

Aqueous solution of glucose (5 M) was investigated. The tissue was immersed in 0.5 ml of the glucose solution and one image stack was acquired every 30 seconds for 6–7 minutes. After the OCA was removed the sample was immersed in 0.1 ml of phosphate buffered saline (PBS), in order to observe the reversibility of the clearing process. The upper limit of tissue shrinkage was estimated as 2% in the course of 6–7 min of OCA application [55].

The average contrast in each image and relative contrast (RC) were defined as [55]

$$\text{Contrast} = \sum_{i,j=1}^{N_{\text{lines}}} \left| I_{i,j} - \left\langle I_{i,j} \right\rangle \right|, \tag{21.15}$$

$$RC = 100 \frac{\text{Contrast}\,[\text{OCA}] - \text{Contrast}\,[\text{PBS}]}{\text{Contrast}\,[\text{PBS}]} \tag{21.16}$$

where $\left\langle I_{i,j} \right\rangle$ is the mean intensity of the nearest eight pixels and $N_{\text{lines}} = N - 2$, with $N = 500$; Contrast[OCA] and Contrast[PBS] are calculated using Eq. (21.15), for OCA and PBS immersion, respectively. Contrast, as defined by Eq. (21.15), is linearly dependent on the fluorescence intensity and varies according to structures in the image. Hence, its usefulness is primarily to enable comparison between images of the same sample at the same depth maintaining the same field of view. Normalization to the total intensity would be required in order to compare different images. The relative contrast RC also serves for the purpose of comparison.

In Ref. [55] it was shown that glucose is effective in improving the image contrast and penetration depth (by up to a factor of two) in two-photon microscopy of *ex vivo* human dermis. Such improvements were obtained within a few minutes of application. For 5M glucose solution RC = 10.9% at 20 μm depth, $\sim$ 134% at 40 μm depth, $\sim$ 471% at 60 μm depth and $\sim$ 406% at 80 μm depth. These data are worst in comparison with both pure glycerol and propylene glycol, but glucose diffuses three times faster than glycerol and five times faster than propylene glycol.

There was found some specificity in action of glucose in comparison with other OCAs. Effects of glucose have not been shown to be reversible. Results presented in Ref. [55] have not demonstrated for glucose a slowing in rate of contrast increase

following addition of PBS rather than a decrease as it was seen for glycerol. Such behavior may be associated with a lesser inclusion of the dehydration mechanism in optical clearing for glucose, and a greater amount of this OCA diffused into a tissue in comparison with glycerol [4].

21.3.3.3 OCT imaging

The typical optical coherence tomography (OCT) fiber optical system employs a broadband light source (a superluminescent diode) to deliver light at a central wavelength of 820 to 1300 nm with a bandwidth of 25-50 nm. Such OCT provides 10–20 μm of axial and transverse resolution in free space with a signal to noise ratio up to 100 dB [116, 117].

For OCT measurements, the intensity of reflected light as a function of the depth z and transverse scanning of the sample is obtained as the magnitude of the digitized interference fringes. The result is the determination of optical backscattering or reflectance, $R(z,x)$, versus the axial ranging distance, or depth, z, and the transverse axis x. The reflectance depends on the optical properties of the tissue or blood, *i.e.*, the absorption (μ_a) and scattering coefficients (μ_s). The relationship between $R(z)$ and attenuation coefficient, $\mu_t = \mu_a + \mu_s$, is, however, very complicated due to the high and anisotropic scattering of tissue and blood, but for optical depths less than four, the reflected power will be approximately proportional to $-2\mu_t z$ on an exponential scale according to the single scattering model [56, 118], and μ_t can be obtained from reflectance measurements at two different depths z_1 and z_2:

$$\mu_t = \frac{1}{2(\Delta z)} \ln\left(\frac{R(z_1)}{R(z_2)}\right), \tag{21.17}$$

where $\Delta z = |z_1 - z_2|$.

A few dozen of repeated scan signals from the sample are usually averaged to estimate the total attenuation coefficient μ_t of the sample. The optical clearing (enhancement of transmittance) ΔT by agents is calculated according to [61]

$$\Delta T = \frac{R_a - R}{R} \times 100\%, \tag{21.18}$$

where R_a is the reflectance from the back surface of the sample with an agent and R that with a control sample.

The OCT images captured from a skin site of a volunteer at a hyperdermal injection of 40%-glucose allowed one to estimate the total attenuation coefficient [see Eq. (21.17)] [62]. The attenuation initially goes down and then over time goes up. Such a behavior correlates well with the spectral measurements shown in Fig. 21.6 and also illustrates the index matching mechanism induced by the glucose injection. The light beam attenuation in tissue, $I/I_0 \sim \exp(-\mu_t)$, for intact skin (0 min) was found from OCT measurements as $I/I_0 \cong 0.14$, and, for immersed skin at 13 min, $I/I_0 \cong 0.30$; *i.e.*, the intensity of the transmitted light increased by 2.1 times. That value also correlates well with the spectral measurements.

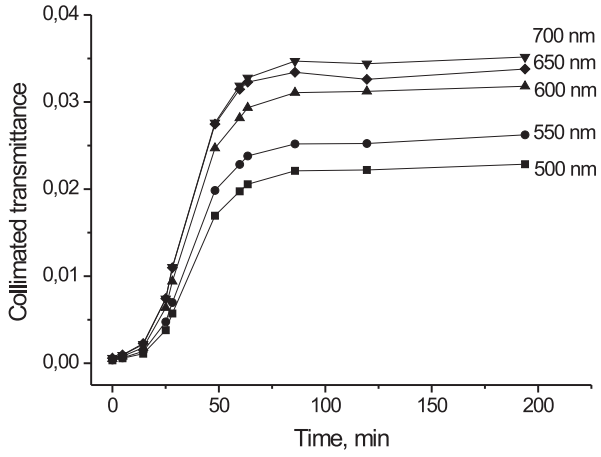

FIGURE 21.5: The time-dependent collimated transmittance of the rat skin sample measured *in vitro* at different wavelengths concurrently with administration of 40%-glucose solution [48].

It should be noted that the high sensitivity of the OCT signal to immersion of living tissue by glucose allows one to monitor its concentration in the skin at a physiological level [25–27].

21.3.3.4 *In vitro* spectral measurements

Figure 21.5 shows the time-dependent collimated transmittance of the rat skin samples measured *in vitro* at different wavelengths concurrently with administration of 40%-glucose solution through dermis, which has fibrous structure [48]. Experimental studies of glucose-induced optical clearing of skin *in vitro* presented in Refs. [44, 47, 48, 51] have demonstrated similarity in kinetics of the process in skin and fibrous tissues as sclera and *dura mater*. However, comparing time of the clearing of skin with data obtained at the clearing of another fibrous tissue, it can be concluded that permeability of the agent into the skin is less than that into the sclera [40, 41, 43] or into the *dura mater* [44, 59, 60]. From Fig. 21.5 it is seen that the glucose solution can effectively control the optical properties of whole skin. At the initial moment the skin is nontransparent for optical radiation. Application of the OCA makes the skin to be more transparent: during 60 min the collimated transmittance increases by more than 30 times at the wavelength 700 nm.

21.3.3.5 *In vivo* spectral and fluorescence measurements

When *in vivo* measurements of skin reflectance are carried out, one needs to exclude influence of SC corneum barrier on the clearing process. To increase efficiency

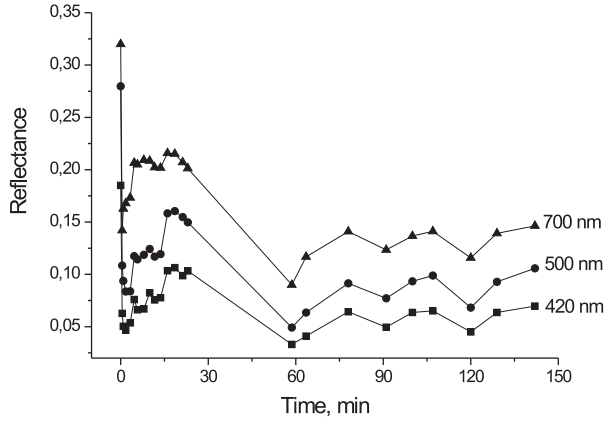

FIGURE 21.6: The time-dependent reflectance of the human skin measured *in vivo* at different wavelengths concurrently with administration of the 40%-glucose solution. The symbols correspond to the experimental data [57].

of OCA permeation through SC, epidermal stripping, electrophoresis or flashlamp-induced micro-damages can be used [58, 119]. For topical application of glucose-gel compositions these methods lead to the enhancement of the kinetics of *in vivo* optical clearing of human skin. For example, application of glucose-gel to skin with removed upper layers of SC gave a rapid 10% drop of reflected light intensity [119].

The administration of glucose solution by intradermal injection is a more effective method. *In vivo* investigations of skin clearing were done with hamsters [47], white rats [44, 48, 51, 57] and male volunteers [49, 51, 57]. As OCAs 40%-glucose solution [44, 48, 51, 57] and highly concentrated glucose (7 M) [47] were used.

Kinetics of reflectance spectra, measured concurrently with intradermal injection of 40%-glucose solution, has shown more than 2-times decreasing of the signal [44, 51]. Figure 21.6 presents kinetics of the human skin reflectance measured at different wavelengths. In the figure it is well seen that immediately after glucose injection the skin reflectance significantly decreases. During the first 20 min the reflectance increases but during the following time interval from 20 to 60 min the skin reflectance decreases again. In the time interval from 60 to 140 min the skin reflectance increases slowly, with oscillating behavior. The reflectance of the skin decreased by about 3.5 times at 700 nm, and then the tissue went slowly back to its normal state.

The significant decreasing of reflectance observed at initial moment is connected with changing geometry of the experiment after glucose injection. The injected solution forms a vesicle filled with the glucose solution in skin, and the vesicle is observed on the skin surface as a swell. Presence of the swell reduces the distance between the collecting fiber and skin surface, decreases area of detection of the back-reflected radiation and hence decreases the reflectance. Injection of the 40%-glucose

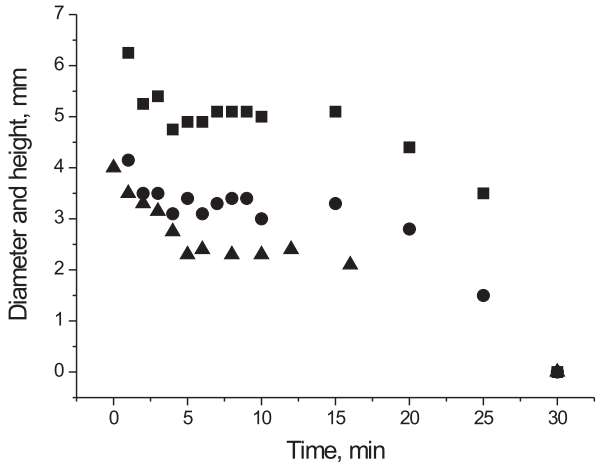

FIGURE 21.7: The changes of skin reaction on injection of 40%-glucose solution. The symbols correspond to the experimental data: bullets — the diameter of virtual transparent window, mm; squares — the diameter of swelling area around the window, mm; triangles — the height of the swell, mm [57].

solution creates the virtual transparent window in skin, which is observed during about 30 min. This window allows one to clearly identify visually blood microvessels in the skin by the naked eye [50, 52]. The swelling white ring appears around the window after the glucose injection. The images of skin were recorded by a digital video camera; diameters of the swelling area and the transparent window were measured [50]. The results are presented in Fig. 21.7.

Assuming that the shape of the vesicle can be presented as an ellipsoid of rotation and taking into account the temporal evolution of the diameter of the swelling area, the height of the swell can be calculated. In 1 min after injection the height is 3.5 mm. During first 5 min after injection the height of the swell decreases to 2.4 mm. In the next 10 min (from 5 to 15 min) the height of the swell does not change. In 30 min after injection the swell on the skin surface disappears.

Schematically the optical clearing at glucose injection can be represented as the following. The clearing agent forms a vesicle filled up with the aqueous solution of glucose in skin dermis. Since skin dermis is elastic porous medium and the glucose solution is incompressible liquid then tissue surrounding the vesicle becomes compressed. Its porosity decreases [120] and ISF is extruded from pores of the dermis. In the initial moment from 0 to 5 min after injection the size of the vesicle decreases significantly under the influence of mechanical pressure of deformed tissue. In the time interval from 5 to 15 min the skin pressure compensates by elastic properties of the glucose solution, and, as a result, the skin reflectance (and size of swell on the

skin surface) does not change [57].

During the time interval from 20 to about 60 min glucose solution diffuses from the vesicle to the surrounding tissue and the corresponding tissue clearing takes place. The glucose-injected region becomes more transparent. Skin scattering decreases and, as consequence of the fact, the reflectance of the skin decreases by about 3.8 times in an hour. Then the reflectance increases gradually, that shows the beginning of glucose diffusion from the observed area and corresponding reduction of tissue immersion. On the basis of the experiments, one can conclude that partial matching of refractive indices of the collagen fibres of dermis and the interstitial medium under action of 40%-glucose solution prevails. It should be noted that the skin was transparent during a few hours. The second phase of tissue interaction with glucose is connected with taking down of the matching effect. It is determined by diffusion of glucose along the skin surface between two cellular layers with a few orders less permeability — epidermal and subdermal fat cells. For the used aperture of the detector system, optical clearing was registered during a few hours [57].

Intradermal injection of glucose influences also the functioning properties of skin, in particular the state of blood microcirculation in dermis. Glucose penetrates vessel walls, interacts with blood cells and leads to local dehydration of tissue and cells [4, 47, 91]. It causes a short-term slowing down and local stasis in different microvessels (arterioles, venules, capillaries), and dilation of microvessels in the area of its application [52].

The effect of glucose has some specific features [52] in comparison with other agents. The degree of dilation of vessels for glucose is larger than that for glycerol. The mean diameter increased by 30% at 30 s after glucose topical application to rat mesentry, and it continued to rise constantly throughout. At the fourth minute it rose by 2.5 fold on average. On the other hand, stasis was maintained in the majority of vessels, but blood flow appeared again in a few of the microvessels from the third to the fifth minute. The velocity of reflow was markedly slower than in controls; throughout the observation the intravascular hemolysis was not seen. There were only aggregates of cells. Individual cells with a clear form in blood aggregates in the lumens of microvessels were found. Vessel walls were registered exactly and, as a whole, after glucose application microvessels were visualized better than in controls (before glucose action) (see Fig. 21.8). The changes in blood flow were also local, but they were observed in a larger area (approximately 1×1 cm^2) in comparison with the glycerol action [52].

It is important to know how the function of blood microvessels changes with decreasing of glucose concentration, *i.e.*, with the loss of its hyperosmolarity. A 30%-glucose solution caused stasis and dilation only in a part of the microvessels. In a few vessels a slowly oscillating blood motion without hemostasis was observed. A 20%-glucose solution also immediately slowed down the blood flow in all microvessels, but stasis is not observed. After 0.5–1.5 s of glucose application the flow rate reduced by half, and it continued to decrease till 20–25th second. From 35 to 40th second the rate in microvessels began to rise. Sometimes reversed shunts can be observed. After 3–4 min of glucose application blood flow in all vessels was not significantly different from the initial one [52].

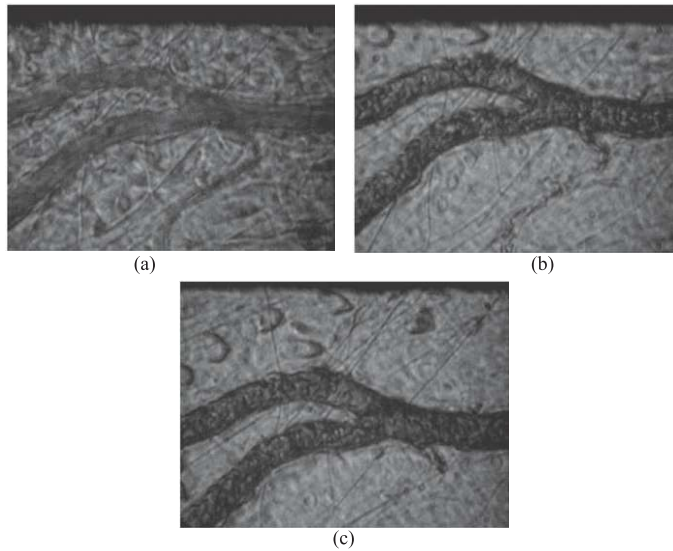

FIGURE 21.8: The effect of 40%-glucose solution on blood microvessels of rat mesentery: (a)—intact state before glucose application (control); (b)—at the 30^{th} second of glucose action; (c)—at the 5^{th} minute of glucose action [52].

Fluorescence measurements were performed for hamster dorsal skin with glucose applied to the subdermal side of the skin and rhodamine fluorescent film placed against the same skin side. Fluorescence was induced by a dye laser pulse at 542 nm delivered to the skin epidermal side by a fiber bundle and was detected by a collection fiber bundle from the epidermal surface at wavelengths longer than 565 nm. On average, up to 100% increase in fluorescence intensity was seen for 20-min glucose application [47].

21.4 Glucose-Induced Optical Clearing Effects in Blood and Cellular Structures

21.4.1 Optical clearing of blood

The main scatterers in blood are RBCs. The major part of this cell is the hemoglobin solution: 90% of the weight of dry RBC is hemoglobin [121]. So the refractive index mismatch between hemoglobin solution in RBC cytoplasm and blood plasma provides strong blood scattering. Intravenous injection of glucose aqueous solutions is widely used in clinical practice [122]; thus optical clearing effects could be ex-

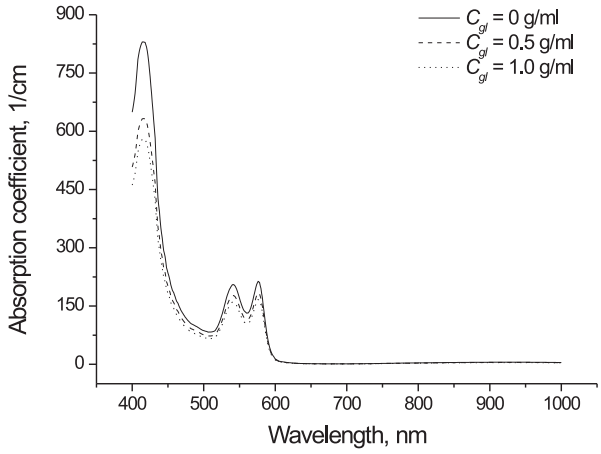

FIGURE 21.9: Absorption spectra of blood at glucose injection calculated in the context of the optical model of blood. The glucose concentration is $C_{\text{gl}} = 0$, 0.5, and 1 g/ml [64].

pected.

Upon introduction of glucose into blood, the refractive index of the blood plasma increases and becomes comparable with that of RBCs. As a consequence, the scattering coefficient decreases, while the blood anisotropy factor increases [65].

The spectral dependence of the refractive index of an aqueous glucose solution is defined by the Eq. (21.5). By analogy with this expression, the refractive index of a glucose solution in the blood plasma can be defined as

$$n_p^{\text{im}}(\lambda) = n_p(\lambda) + 0.1515 C_{\text{gl}}, \tag{21.19}$$

where $n_p(\lambda)$ is the refractive index of the blood plasma defined by Eq. (21.11).

A change in the osmolarity of the plasma leads to changes in the size and the complex refractive index of RBCs due to their osmotic dehydration [91] and, consequently, to changes in their scattering and absorption properties. Normally, the osmolarity of blood amounts to 280–300 mosm/l [91]. The introduction of glucose into the blood plasma leads to a linear increase in the osmolarity, which reaches the value 6000 mosm/l at a glucose concentration in the blood plasma of about 1 g/ml. At introduction of glucose into the blood plasma, the hematocrit of the blood decreases.

The osmotic dehydration leads to an increase in the concentration of hemoglobin in blood and, as a consequence, to an increase in both the real and the imaginary parts of the refractive index of RBCs. The changes in the real and imaginary parts of the refractive index were estimated using Eqs. (21.9) and (21.10) and account for the change in the hemoglobin concentration defined by Eq. (21.8).

The absorption and reduced scattering coefficients and anisotropy factor of whole

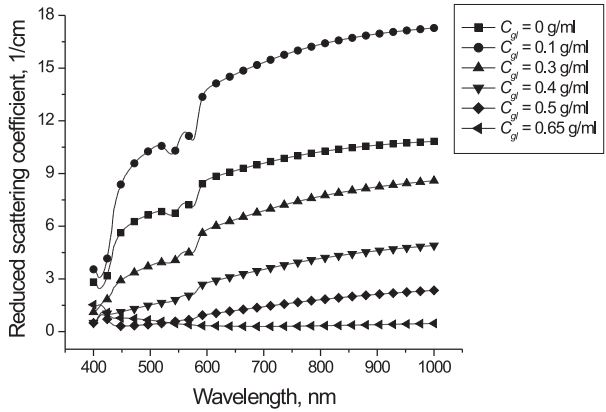

FIGURE 21.10: Calculated spectra of the transport scattering coefficient of blood at glucose injection. $C_{gl} = 0$, 0.1, 0.3, 0.4, 0.5, and 0.65 g/ml [64].

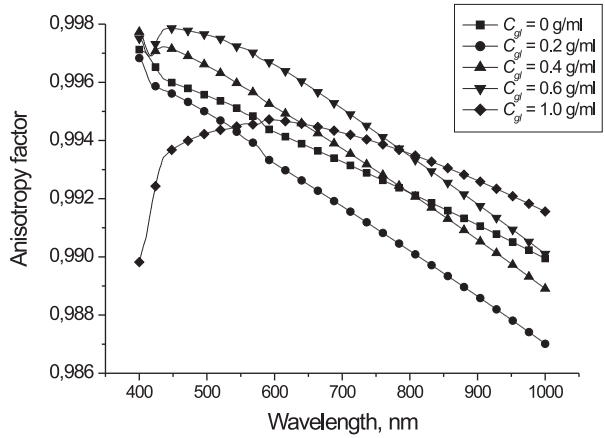

FIGURE 21.11: Calculated spectral dependence of the scattering anisotropy factor of blood at glucose injection. C_{gl} = 0, 0.2, 0.4, 0.6, and 1.0 g/ml [64].

blood at glucose injection (see Figs. 21.9–21.11) were calculated on the basis of optical model of blood [see Eqs. (21.12)–(21.14)]. Maximal optical clearing is observed at a glucose concentration of 0.65 g/ml [64].

21.4.2 Time-domain and frequency-domain measurements

The kinetic response of optical properties of blood, cell suspensions and tissue treated by glucose was measured using a time-domain and frequency-domain techniques [37–39, 63]. The waves in the near infrared (816, 830 and 850 nm) were used. Time-resolved spectroscopy is effective for measuring the optical properties of highly scattering medium; the frequency-domain can give a transient response of mean path length change [122, 123]. Intensity and phase of photon density waves are measured at several source-detector separations.

21.4.3 Experimental results

For the noninvasive *in vivo* measurement the response of a nondiabetic male subject to a glucose load of 1.75 g/kg body weight, as in a standard glucose tolerance test, was used by continuously monitoring the product $n\mu_s'$ measured on muscle tissue of the subject's thigh [63]. The values of blood glucose concentrations lay in physiological range 80–150 mg/dL. The correlation between the blood glucose as measured with the home blood glucose monitor with the measured product $n\mu_s'$ was indicated. An increase of glucose concentration in the physiological range decreases the total amount of tissue scattering [68].

A number of studies deals with the control of scattering properties of cellular tissues such as liver [37–39] and cell cultures and phantoms [37, 68, 88] using aqueous glucose solutions. It was demonstrated that light scattering of the rat liver results mainly from both the whole hepatocyte volume and the intracellular organelles, including mitochondria [37–39, 123]. Those studies suggested that mitochondria are the major source for light scattering in tissue by showing that about 85% of the reduced scattering of the liver originates from mitochondria. In living tissue light scattering depends not only from the extracellular refractive index (n_{ex}) but also from the intracellular refractive index (n_{in}) and cell size upon exposure to osmotic pressure. If additions of OCAs are involved, one may encounter multiple effects due to changes in cell size and in cellular refractive indexes [37–39].

The addition of glucose solution into tissue can cause both a decrease in cell volume and an increase in refractive index of the extracellular fluid. These two changes contradict each other in the overall scattering behavior of the tissue. The effect of an increase of extracellular refractive index is larger, giving an overall decrease in μ_s'. However, if the intracellular refractive index also increases when the added glucose permeates to the cells, the change of cell size becomes the major factor since the effects of intra- and extracellular refractive indexes cancel one another. Specifically, in the liver glucose perfusion measurements represented by Ref. [39], the mean path length of the perfused liver increased rapidly and then returned to its original value within 2 to 3 min. This increase in path length indicates that: (1) glucose may enter the cells and result in increases of both n_{in} and n_{ex} so that the effect of changes in refractive indexes is relatively small, and (2) a decrease in cell size and cell volume fraction must occur in the beginning of the perfusion, leading to an increase in path length and μ_s', but soon the shrunken cells regain some of their original volumes [39].

Thus, addition of glucose solution to cellular suspension and tissue affects the size of cells and the refractive indices of extra- and intracellular fluid, and thus affects the overall tissue scattering properties.

21.5 Conclusion

This chapter shows that glucose administration in tissues and blood allows one to control effectively its optical properties. Such control leads to the essential reduction of scattering and therefore causes much higher transmittance (optical clearing) and the appearance of a large amount of least-scattered and ballistic photons, allowing for successful applications of different imaging techniques for medicine. The kinetics of tissue optical clearing, defined, in general, by both the kinetics of dehydration and refractive index matching, is characterized by different time intervals in dependence on tissue and used agents. The swelling or shrinkage of the tissue and cells under action of clearing agents may play an important role in the tissue clearing process. Along with common features in character of tissue clearing under action of immersion agent, glucose has a number of peculiarities in its influence on tissues and blood.

The immersion technique has a great potential for noninvasive medical diagnostics using reflectance spectroscopy, frequency-domain measurements, OCT, confocal microscopy and other methods where scattering is a serious limitation. Optical clearing can increase effectiveness of a number of therapeutic and surgical methods using laser action on a target area hindered in depth of a tissue.

Acknowledgment

This work has been supported in part by grants PG05-006-2 and REC-006 of U.S. Civilian Research and Development Foundation for the Independent States of the Former Soviet Union (CRDF) and the Russian Ministry of Science and Education, and grant of RFBR No. 06-02-16740-a.

References

[1] N. Kollias and G. N. Stamatas, "Optical non-invasive approaches to diagnosis of skin diseases," *Oct. JID Symp. Proc.,* vol. 7, 2002, pp. 64-75.

[2] J.G. Fujimoto and M.E. Brezinski, "Optical coherence tomography imaging," in *Biomedical Photonics Handbook*, ed. T. Vo-Dinh, Chap. 13, CRC Press LLC, Boca Raton, 2003.

[3] M.C. Pierce, J. Strasswimmer, B.H. Park, et al., "Advances in optical coherence tomography imaging for dermatology," *J. Invest. Dermatol.,* vol. 123, 2004, pp. 458-463.

[4] V.V. Tuchin, *Tissue Optics: Light Scattering Methods and Instruments for Medical Diagnosis*, vol. PM 166, SPIE Press, Bellingham, WA, 2007.

[5] I.J. Bigio and J.R. Mourant, "Ultraviolet and visible spectroscopies for tissue diagnostics: fluorescence spectroscopy and elastic-scattering spectroscopy," *Phys. Med. Biol.,* vol. 42, 1997, pp. 803-814.

[6] P. Thueler, I. Charvet, F. Bevilacqua, et al., "*In vivo* endoscopic tissue diagnostics based on spectroscopic absorption, scattering, and phase function properties," *J. Biomed. Opt.,* vol. 8, 2003, pp. 495-503.

[7] V.P. Zharov, S. Ferguson, J.F. Eidt, et al., "Infrared imaging of subcutaneous veins," *Lasers Surg. Med.,* vol. 34, 2004, pp.56-61.

[8] S. Andersson-Engels, C. Klinteberg, K. Svanberg, and S. Svanberg, "*In vivo* fluorescence imaging for tissue diagnostics," *Phys. Med. Biol.,* vol. 42, 1997, pp. 815-824.

[9] S.L. Jacques, J.C. Ramella-Roman, and K. Lee, "Imaging skin pathology with polarized light," *J. Biomed. Opt.,* vol. 7, 2002, pp. 329-340.

[10] A.N. Yaroslavsky, V. Neel, and R.R. Anderson, "Demarcation of nonmelanoma skin cancer margins in thick excisions using multispectral polarized light imaging," *J. Invest. Dermatol*., vol. 121, 2003, pp. 259-266.

[11] V.V. Tuchin (ed.), *Handbook of Optical Biomedical Diagnostics,* vol. PM107, SPIE Press, Bellingham, WA, 2002.

[12] D.A. Boas, M.A. Franceschini, A.K. Dunn, and G. Strangman, "Noninvasive imaging of cerebral activation with diffuse optical tomography," in: *In Vivo Optical Imaging of Brain Function*, R. D. Frostig (ed.), CRC Press LLC, Boca Raton, 2002, pp. 193-221.

[13] E. Gratton, V. Toronov, U. Wolf, M. Wolf, and A. Webb, "Measurement of brain activity by near-infrared light," *J. Biomed. Opt.,* vol. 10, 2005, 011008.

[14] C.S. Robertson, S.P. Gopinath, and B. Chance, "A new application for near-infrared spectroscopy: detection of delayed intracranial hematomas after head injury," *J. Neurotrauma (Suppl.),* vol. 12, 1995, pp. 591-600.

[15] F. Bevilacqua, D. Piguet, P. Marquet, J.D. Gross, B.J. Tromberg, and C. Depeursinge, "*In vivo* local determination of tissue optical properties: applications to human brain," *Appl. Opt.* vol. 38, 1999, pp. 4939-4950.

[16] W.-C. Lin, S.A. Toms, M. Johnson, E.D. Jansen, and A. Mahadevan-Jansen, "*In vivo* brain tumor demarcation using optical spectroscopy," *Photochem. Photobiol.*, vol. 73, 2001, pp. 396-402.

[17] W.A. Kalender, "X-ray computed tomography," *Phys. Med. Biol.*, vol. 51, 2006, pp. R29-R43.

[18] Y. Chen, D.R. Tailor, X. Intes, and B. Chance, "Correlation between near-infrared spectroscopy and magnetic resonance imaging of rat brain oxygenation modulation," *Phys. Med. Biol.*, vol. 48, 2003, pp. 417-427.

[19] A.M. Siegel, J.P. Culver, J.B. Mandeville, and D.A. Boas, "Temporal comparison of functional brain imaging with diffuse optical tomography and fMRI during rat forepaw stimulation," *Phys. Med. Biol.*, vol. 48, 2003, pp. 1391-1403.

[20] X. Wang, Y. Pang, G. Ku, X. Xie, G. Stoica, and L.V. Wang, "Noninvasive laser-induced photoacoustic tomography for structural and functional in vivo imaging of the brain," *Nature Biotechnol.*, vol. 21, 2003, pp. 803-806.

[21] A.J. du Plessis and J.J. Volpe, "Cerebral oxygenation and hemodynamic changes during infant cardiac surgery: measurements by near infrared spectroscopy," *J. Biomed. Opt.*, vol. 1, 1996, pp. 373-386.

[22] S. Fantini, E.L. Heffer, V.E. Pera, A. Sassaroli, and N. Liu, "Spatial and spectral information in optical mammography," *Technol. Cancer Res. Treat.*, vol. 4, 2005 pp. 471-482.

[23] A. Gerger, S. Koller, T. Kern, et al., "Diagnostic applicability of *in vivo* confocal laser scanning microscopy in melanocytic skin tumors," *J. Invest. Dermatol.*, vol. 124, 2005, pp. 493-498.

[24] B.R. Masters and P.T.C. So, "Confocal microscopy and multi-photon excitation microscopy of human skin in vivo," *Opt. Express*, vol. 8, 2001, pp. 2-10.

[25] P.J. Campagnola, H.A. Clark, W.A. Mohler, A. Lewis, and L.M. Loew, "Second-harmonic imaging microscopy of living cells," *J. Biomed. Opt.*, vol. 6, 2001, pp. 277-286.

[26] K.V. Larin, M.S. Eledrisi, M. Motamedi, and R.O. Esenaliev, "Noninvasive blood glucose monitoring with optical coherence tomography," *Diabetes Care*, vol. 25, 2002, pp. 2263-2267.

[27] K.V. Larin, M. Motamedi, T.V. Ashitkov, and R.O. Esenaliev, "Specificity of noninvasive blood glucose sensing using optical coherence tomography technique: a pilot study," *Phys. Med. Biol.*, vol. 48, 2003, pp. 1371-1390.

[28] O.S. Khalil, "Non-invasive glucose measurement technologies: an update from 1999 to the dawn of the new millennium," *Diabet. Technol. Ther.*, vol. 6, 2004, pp. 660-697.

[29] A. Douplik, A.A. Stratonnikov, V.B. Loshchenov, et al., "Study of photodynamic reactions in human blood," *J. Biomed. Opt.*, vol. 5, 2000, pp. 338-349.

[30] M.A. Calin and S.V. Parasca, "Photodynamic therapy in oncology," *J. Optoelectr. Adv. Mater.*, vol. 8, 2006, pp. 1173-1179.

[31] G. Müller and A. Roggan (eds.), *Laser–Induced Interstitial Thermotherapy*, vol. PM25, SPIE Press, Bellingham, WA, 1995.

[32] K. Orth, D. Russ, J. Duerr, R. Hibst, R. Steiner, and G.H. Beger, "Thermocontrolled device for inducing deep coagulation in the liver with the Nd:YAG laser," *Lasers Surg. Med.*, vol. 20, 1997, pp. 149-156.

[33] B.J. Zuger, B. Ott, P. Mainil-Varlet, et al., "Laser solder welding of articular cartilage: tensile strength and chondrocyte viability," *Lasers Surg. Med.*, vol. 28, 2001, pp. 427-434.

[34] Z.S. Sacks, R.M. Kurtz, T. Juhasz, and G.A. Mourau, "High precision subsurface photodistribution in human sclera," *J. Biomed. Opt.*, vol. 7, 2002, pp. 442-450.

[35] P.-Ch. Kuo, G. A. Peyman, G. Men, Y. Bezerra, and F. Torres, "The effect of indocyanine green pretreatment on the parameters of transscleral diode laser thermotherapy-induced threshold coagulation of the ciliary body," *Lasers Surg. Med.*, vol. 35, 2004, pp. 157-162.

[36] J.M. Schmitt and G. Kumar, "Optical scattering properties of soft tissue: a discrete particle model," *Appl. Opt.*, vol. 37, 1998, pp. 2788-2797.

[37] B. Beauvoit, T. Kitai, and B. Chance, "Contribution of the mitochondrial compartment to the optical properties of rat liver: a theoretical and practical approach," *Biophys. J.*, vol. 67, 1994, pp. 2501-2510.

[38] B. Chance, H. Liu, T. Kitai, et al., "Effects of solutes on optical properties of biological materials: models, cells, and tissues," *Anal. Biochem.*, vol. 227, 1995, pp. 351-362.

[39] H. Liu, B. Beauvoit, M. Kimura, et al., "Dependence of tissue optical properties on solute-induced changes in refractive index and osmolarity," *J. Biomed. Opt.*, vol. 1, 1996, pp. 200-211.

[40] V.V. Tuchin, I.L. Maksimova, D.A. Zimnyakov, et al., "Light propagation in tissues with controlled optical properties," *J. Biomed. Opt.*, vol. 2, 1997, pp. 401-417.

[41] V.V. Tuchin, A.N. Bashkatov, E.A. Genina, and Yu.P. Sinichkin, "Scleral tissue clearing effects," *Proc SPIE* 4611, 2002, pp. 54-58.

[42] A.N. Bashkatov, V.V. Tuchin, E.A. Genina, et al., "The human sclera dynamic spectra: *in-vitro* and *in-vivo* measurements," *Proc SPIE* 3591, 1999, pp. 311-319.

[43] A.N. Bashkatov, E.A. Genina, V.I. Kochubey, et al., "Osmotical liquid diffusion within sclera," *Proc SPIE* 3908, 2000, pp. 266-276.

[44] A.N. Bashkatov, E.A. Genina, and V.V. Tuchin, "Optical immersion as a tool for tissue scattering properties control," in *Perspectives in Engineering Optics*, K. Singh and V.K. Rastogi (eds.), Anita Publications, New Delhi, India, 2002, pp. 313-334.

[45] A.N. Bashkatov, E.A. Genina, Yu.P. Sinichkin, et al., "Estimation of the glucose diffusion coefficient in human eye sclera," *Biophys.*, vol. 48, 2003, pp. 292-296.

[46] E.A. Genina, A.N. Bashkatov, Yu.P. Sinichkin, et al., "Optical clearing of the eye sclera *in vivo* caused by glucose," *Quant. Electr.*, vol. 36, 2006, pp. 1119-1124.

[47] G. Vargas, K.F. Chan, S.L. Thomsen, et al., "Use of osmotically active agents to alter optical properties of tissue: effects on the detected fluorescence signal measured through skin," *Lasers Surg. Med.*, vol. 29, 2001, pp. 213-220.

[48] A.N. Bashkatov, E.A. Genina, I.V. Korovina, et al., "*In vivo* and *in vitro* study of control of rat skin optical properties by action of 40%-glucose solution," *Proc SPIE* 4241, 2001, pp. 223-230.

[49] V.V. Tuchin, A.N. Bashkatov, E.A. Genina, et al., "*In vivo* investigation of the immersion-liquid-induced human skin clearing dynamics," *Techn. Phys. Lett.*, vol. 27, 2001, pp. 489-490.

[50] E.I. Galanzha, V.V. Tuchin, Q. Luo, et al., "The action of osmotically active drugs on optical properties of skin and state of microcirculation in experiments," *Asian J. Phys.*, vol. 10, 2001, pp. 503-511.

[51] E.A. Genina, A.N. Bashkatov, I.V. Korovina, et al., "Control of skin optical properties: *in vivo* and *in vitro* study," *Asian J. Phys.*, vol. 10, 2001, pp. 493-501.

[52] E.I. Galanzha, V.V. Tuchin, A.V. Solovieva, et al., "Skin backreflectance and microvascular system functioning at the action of osmotic agents," *J. Phys. D: Appl. Phys.*, vol. 36, 2003, pp. 1739-1746.

[53] I.V. Meglinskii, A.N. Bashkatov, E.A. Genina, et al., "Study of the possibility of increasing the probing depth by the method of reflection confocal microscopy upon immersion clearing of near-surface human skin layers," *Quant. Electr.*, vol. 32, 2002, pp. 875-882.

[54] I.V. Meglinski, A.N. Bashkatov, E.A. Genina, D.Y. Churmakov, and V.V. Tuchin, "The Enhancement of Confocal Images of Tissues at Bulk Optical Immersion," *Laser Phys.*, vol. 13, 2003, pp. 65–69.

[55] R. Cicchi, F.S. Pavone, D. Massi, et al., "Contrast and depth enhancement in two-photon microscopy of human skin *ex vivo* by use of clearing agents," *Opt. Express*, vol. 13, 2005, pp. 2337-2344.

[56] V.V. Tuchin, "Optical immersion as a new tool for controlling the optical properties of tissues and blood," *Laser Phys.*, vol. 15, 2005, pp. 1109-1136.

[57] A.N. Bashkatov, A.N. Korolevich, V.V. Tuchin, et al., "*In vivo* investigation of human skin optical clearing and blood microcirculation under the action of glucose solution," *Asian J. Phys.*, vol. 15, 2006, pp. 1-14.

[58] V.V. Tuchin, G.B. Altshuler, A.A. Gavrilova, et al., "Optical clearing of skin using flashlamp-induced enhancement of epidermal permeability," *Lasers Surg. Med.*, vol. 38, 2006, pp. 824-836.

[59] L. Yao, H. Cheng, Q. Luo, et al., "Control of rabbit *dura mater* optical properties with osmotical liquids," *Proc SPIE* 4536, 2002, pp. 147-152.

[60] A.N. Bashkatov, E.A. Genina, Yu.P. Sinichkin, et al., "Glucose and mannitol diffusion in human *dura mater*," *Biophys. J.*, vol. 85, 2003, pp. 3310-3318.

[61] V.V. Tuchin, X. Xu, and R. K. Wang, "Dynamic optical coherence tomography in studies of optical clearing, sedimentation, and aggregation of immersed blood," *Appl. Opt.*, vol. 41, 2002, pp. 258-271.

[62] R.K. Wang and V.V. Tuchin, "Enhance light penetration in tissue for high resolution optical imaging techniques by the use of biocompatible chemical agents," *J. X-Ray Sci. Technol.*, vol. 10, 2002, pp. 167-176.

[63] J.S. Maier, S.A. Walker, S. Fantini, et al., "Possible correlation between blood glucose concentration and the reduced scattering coefficient of tissues in the near infrared," *Opt. Lett.*, vol. 19, 1994, pp. 2062-2064.

[64] A.N. Bashkatov, D.M. Zhestkov, E.A. Genina, et al., "Immersion clearing of human blood in the visible and near-infrared spectral regions," *Opt. Spectr.*, vol. 98, 2005, pp. 638-646.

[65] V.V. Tuchin, *Optical Clearing in Tissues and Blood*, SPIE Optical Engineering Press, Bellingham, WA, 2005.

[66] Y. Komai and T. Ushiki, "The three-dimensional organization of collagen fibrils in the human cornea and sclera," *Invest. Ophthal. Vis. Sci.*, vol. 32, 1991, pp. 2244-2258.

[67] I.S. Saidi, S.L. Jacques, and F.K. Tittel, "Mie and Rayleigh modeling of visible-light scattering in neonatal skin," *Appl. Opt.*, vol. 34, 1995, pp. 7410-7418.

[68] V.I. Zyablov, Yu.N. Shapovalov, K.D. Toskin, et al., "Structure and physicomechanical properties of human *dura mater* in age-specific aspect," *Arch. Anat., Histol. Embryol. (Russia),* vol. 3, 1982, pp. 29-36.

[69] E.M. Culav, C.H. Clark, and M.J. Merrilees, "Connective tissue: matrix composition and its relevance to physical therapy," *Phys. Ther.*, vol. 79, 1999, pp. 308-319.

[70] R.L. Jackson, S.J. Busch, and A.D. Cardin, "Glycosaminoglycans: molecular properties, protein interactions, and role in physiological processes," *Physiol. Rev.*, vol. 71, 1991, pp. 481-539.

[71] O.A. Boubriak, J.P.G. Urban, S. Akhtar, et al., "The effect of hydration and matrix composition on solute diffusion in rabbit sclera," *Exp. Eye Res.*, vol. 71, 2000, pp. 503-514.

[72] P.O. Rol, *Optics for Transscleral Laser Applications*, *PhD Thesis*, Swiss Federal Institute of Technology, Zurich, Switzerland, 1991.

[73] S. Vaezy and J.I. Clark, "Quantitative analysis of the microstructure of the human cornea and sclera using 2-D Fourier methods," *J. Microsc.*, vol. 175, 1994, pp. 93-99.

[74] M.A. Baron and N.A. Mayorova, *Atlas of Functional Stereomorphology of Brain Membranes*, Medicine, Moscow, 1982.

[75] H. Schaefer and T.E.Redelmeier, *Skin Barrier*, Karger, Basel et al., 1996.

[76] G.F. Odland, "Structure of the skin," in *Physiology, Biochemistry and Molecular Biology of the Skin,* L.A. Goldsmith (ed.), Oxford University Press, Oxford, vol. 1, 1991, pp. 3-62.

[77] T.J. Ryan, "Cutaneous circulation," in *Physiology, Biochemistry, and Molecular Biology of the Skin*, L.A. Goldsmith (ed.), Oxford University Press, Oxford, vol. 2, 1991, pp. 1019-1084.

[78] K.S. Stenn, "The skin," in *Cell and Tissue Biology*, L. Weiss (ed.), Urban & Shwarzenberg, Baltimore, 1988, pp. 541-572.

[79] A.R. Young, "Chromophores in human skin," *Phys. Med. Biol.*, vol. 42, 1997, pp. 789-802.

[80] M.R. Chedekel, "Photophysics and photochemistry of melanin," in: *Melanin: Its Role in Human Photoprotection*, L. Zeise, M.R. Chedekel, and T.B. Fitzpatrick (eds.), Valdenmar, Overland Park, 1995, pp. 11-22.

[81] A. Zourabian, A. Siegel, B. Chance, et al., "Trans-abdominal monitoring of fetal arterial blood oxygenation using pulse oximetry," *J. Biomed. Opt.*, vol. 5, 2000, pp. 391-405.

[82] T. Hamaoka, T. Katsumura, N. Murase, et al., "Quantification of ischemic muscle deoxygenation by near infrared time-resolved spectroscopy," *J. Biomed. Opt.*, vol. 5, 2000, pp. 102-105.

[83] J. Mobley and T. Vo-Dinh, "Optical properties of tissue," in *Biomedical Photonics Handbook*, T. Vo-Dinh (ed.), Chap. 2, CRC Press LLC, Boca Raton, 2003.

[84] J.L. Cox, R.A. Farrell, R.W. Hart, et al., "The transparency of the mammalian cornea," *J. Physiol.*, vol. 210, 1970, pp. 601-616.

[85] C.F. Bohren and D.R. Huffman, *Absorption and Scattering of Light by Small Particles*, Wiley, New York, 1983.

[86] D.E. Freund, R.L. McCally, and R.A. Farrell, "Effects of fibril orientations on light scattering in the cornea," *J. Opt. Soc. Am. A*., vol. 3, 1986, pp. 1970-1982.

[87] D.W. Leonard and K.M. Meek, "Refractive indices of the collagen fibrils and extrafibrillar material of the corneal stroma," *Biophys. J.*, vol. 72, 1997, pp. 1382-1387.

[88] M. Kohl, M. Esseupreis, and M. Cope, "The influence of glucose concentration upon the transport of light in tissue-simulating phantoms," *Phys. Med. Biol.*, vol. 40, 1995, pp. 1267-1287.

[89] Y. Huang and K.M. Meek, "Swelling studies on the cornea and sclera: the effects of pH and ionic strength," *Biophys. J.*, vol. 77, 1999, pp. 1655-1665.

[90] I.V. Meglinski and S.J. Matcher, "Quantitative assessment of skin layers absorption and skin reflectance spectra simulation in visible and near-infrared spectral region," *Physiol. Measur.,* vol. 23, 2002, pp. 741-753.

[91] A. Roggan, M. Friebel, K. Dorschel, et al., "Optical properties of circulating human blood in the wavelength range 400-2500 nm," *J. Biomed. Opt.*, vol. 4, 1999, pp. 36-46.

[92] A.G. Borovoi, E.I. Naats, and U.G. Oppel, "Scattering of light by a red blood cell," *J. Biomed. Opt.*, vol. 3, 1998, pp. 364-372.

[93] M.Yu. Kirillin and A.V. Priezzhev, "Monte Carlo simulation of laser beam propagation in a plane layer of the erythrocytes suspension: comparison of contributions from different scattering orders to the angular distribution of light intensity," *Quant. Electr.*, vol. 32, 2002, pp. 883-887.

[94] M. Hammer, D. Schweitzer, B. Michel, et al., "Single scattering by red blood cells," *Appl. Opt.*, vol. 37, 1998, pp. 7410-7418.

[95] D.H. Tycko, M.H. Metz, E.A. Epstein, et al., "Flow-cytometric light scattering measurement of red blood cell volume and hemoglobin concentration," *Appl. Opt.*, vol. 24, 1985, pp. 1355-1365.

[96] V.A. Levtov, S.A. Regirer, and I.Kh. Shadrina, *Rheology of Blood*, Medicine, Moscow, 1982.

[97] A.V. Priezzhev, O.M. Ryaboshapka, N.N. Firsov, and I.V. Sirko, "Aggregation and disaggregation of erythrocytes in whole blood: study by backscattering technique," *J. Biomed. Opt.*, vol. 4, 1999, pp. 76-84.

[98] N.G. Khlebtsov and S.Yu. Shchegolev, "Account of particles nonsphericity at determination of parameters of dispersion systems by a turbidity spectrum method. I. Characteristic functions of light scattering by systems of randomly oriented nonspherical particles in Rayleigh-Gans approximation," *Opt. Spectr.,* vol. 42, 1977, pp. 549-555.

[99] N.G. Khlebtsov and S.Yu. Shchegolev, "Account of particles nonsphericity at determination of parameters of dispersion systems by a turbidity spectrum method. II. Characteristic functions of light scattering by systems of randomly oriented nonspherical particles in van de Hulst approximation," *Opt. Spectr.,* vol. 42, 1977, pp. 663-668.

[100] S. Cheng, H. Y. Shen, G. Zhang, C. H. Huang, X. J. Huang, "Measurement of the refractive index of biotissue at four laser wavelengths," *Proc SPIE*, vol. 4916, 2002, pp. 172-176.

[101] A.N. Yaroslavsky, A.V. Priezzhev, J. Rodriguez, I.V. Yaroslavsky, and H. Battarbee, "Optics of blood," in *Handbook of Optical Biomedical Diagnostics,* V.V. Tuchin (ed.), vol. PM107, SPIE Press, Bellingham, WA, 2002, p. 169.

[102] V.S. Lee and L. Tarassenko, "Absorption and multiple scattering by suspensions of aligned red blood cells," *J. Opt. Soc. Am. A*, vol. 8, 1991, pp. 1135-11416.

[103] C.G. Rylander, O.F. Stumpp, T.E. Milner, et al., "Dehydration mechanism of optical clearing in tissue," *J. Biomed. Opt.*, vol. 11, 2006, 041117.

[104] A.T. Yeh and J. Hirshburg, "Molecular interactions of exogenous chemical agents with collagen-implications for tissue optical clearing," *J. Biomed. Opt.*, vol. 11, 2006, 014003.

[105] A.T. Yeh, B. Choi, J.S. Nelson, and B.J. Tromberg, "Reversible dissociation of collagen in tissues," *J. Invest. Dermatol.*, vol. 121, 2003, pp. 1332-1335.

[106] S. Plotnikov, V. Juneja, A.B. Isaacson, W.A. Mohler, and P.J. Campagnola, "Optical clearing for improved contrast in second harmonic generation imaging of skeletal muscle," *Biophys. J.*, vol. 90, 2006, pp. 328-339.

[107] S.A. Prahl, M.J.C. van Gemert, and A.J. Welch, "Determining the optical properties of turbid media by using the adding-doubling method," *Appl. Opt.*, vol. 32, 1993, pp. 559-568.

[108] M. Hammer, A. Roggan, D. Schweitzer, and G. Muller, "Optical properties of ocular fundus tissues – an *in vitro* study using the double-integrating-sphere technique and inverse Monte Carlo simulation," *Phys. Med. Biol.*, vol. 40, 1995, pp. 963-978.

[109] D.A. Zimnyakov and Yu.P. Sinichkin, "A study of polarization decay as applied to improved imaging in scattering media," *J. Opt. A: Pure Appl. Opt*. vol. 2, 2000, pp. 200-208.

[110] T.R. Mollee and A.J. Bracken, "A model of solute transport through stratum corneum using solute capture and release," *Bull. Math. Biol.*, vol. 69, 2007, pp. 1887–1907.

[111] A.-H. Ghanem, H. Mahmoud, W.I. Higuchi, P. Liu, and W.R. Good, "The effects of ethanol on the transport of lipophilic and polar permeants across hairless mouse skin: Methods/validation of a novel approach," *Int. J. Pharm.*, vol. 78, 1992, pp. 137-156.

[112] G.F. Odland, *Physiology, Biochemistry and Molecular Biology of the Skin*, L. A. Goldsmith (ed.), Oxford University Press, Oxford, vol. 1, 1991, p.3.

[113] W. Denk, J.H. Strickler, and W.W. Webb, "Two-photon laser scanning fluorescence microscope," *Science*, vol. 248, 1990, pp. 73-76.

[114] A.K. Dunn, V.P. Wallace, M. Coleno, M.W. Berns, and B.J. Tromberg, "Influence of optical properties on two-photon fluorescence imaging in turbid samples," *Appl. Opt.*, vol. 39, 2000, pp. 1194-1201.

[115] M. Gu, X. Gan, A. Kisteman, and M. G. Xu, "Comparison of penetration depth between two-photon excitation and single-photon excitation in imaging through turbid tissue media," *Appl. Phys. Lett.*, vol. 77, 2000, pp. 1551-1553.

[116] B.E. Bouma and G.J. Tearney, *Handbook of Optical Coherence Tomography,* Marcel-Dekker, New York, 2002.

[117] V.V. Tuchin, *Coherent-Domain Optical Methods for Biomedical Diagnostics, Environmental and Material Science,* Kluwer, Boston, 2004.

[118] R.K. Wang and V.V. Tuchin, *Coherent-Domain Optical Methods: Biomedical Diagnostics, Environmental and Material Science*, by V.V. Tuchin (ed.), Kluwer Academic Publishers, Boston, 2004.

[119] S.P. Chernova, N.V. Kuznetsova, A.B. Pravdin, and V.V. Tuchin, "Dynamics of optical clearing of human skin *in vivo*," *Proc SPIE* 4162, 2000 pp. 227-235.

[120] R.E. Collins, *Flow of Fluids through Porous Materials,* Reinhold Publishing Corporation, New York, 1961.

[121] R.F. Schmidt and G. Thews, *Human Physiology,* Springer, Berlin, 1989.

[122] H. Liu, M. Miwa, B. Beauvoit, N.G. Wang, and B. Chance, "Characterization of absorption and scattering properties of small-volume biological samples using time-resolved spectroscopy," *Anal. Biochem.,* vol. 213, 1993, pp. 378–385.

[123] S. Fantini, M.A. Franceschini-Fantini, J.S. Maier, S.A. Walker, B. Barbieri, and E. Gratton, "Frequency-domain multichannel optical detector for noninvasive tissue spectroscopy and oximetry," *Opt. Eng.*, vol. 34, 1995, pp. 32–42.